Quantum chaos on ordered structures by scattering techniques: Application to low-energy electron diffraction

P. L. de Andres and J. A. Vergés
Instituto de Ciencia de Materiales de Madrid, Consejo Superior de Investigaciones Científicas, Cantoblanco, E-28049 Madrid, Spain
(Received 23 June 1998; revised manuscript received 20 August 1998)

We analyze statistical probability distributions of intensities collected using diffraction techniques such as low-energy electron diffraction (LEED). A simple theoretical model based on hard-sphere potentials and LEED formalism is investigated for different values of relevant parameters: energy, angle of incidence, muffin-tin-potential radius, maximum spherical component l_{max}, number of stacked layers, and full multiple-scattering or kinematic model. Given a complex enough system (e.g., including multiple scattering by at least two Bravais lattices), the computed probability distributions agree rather well with a χ_2^2 one, characteristic of the Gaussian unitary ensemble universality class associated with quantum chaos. A hypothesis on the possible impact of the chaotic nature of wave functions on correlation factors is tested against the behavior of the Pendry R factor and the root mean square deviation factor. [S0163-1829(99)00804-8]

I. INTRODUCTION

There is much interest in the role of chaos on quantum systems. The important consequences of chaos on classical systems motivate extending the study of chaos to the quantum physics world. It is difficult, however, to explore quantum chaos by connecting the quantum and classical formulation using special limits.[1] Therefore, a group of pioneering investigators adopted a long time ago a point of view independent of any classical or semiclassical approach to chaos.[2] In this approach the object of interest is a Hamiltonian composed of random numbers [random matrix theory (RMT)],[3,4] conjectured by Wigner, Dyson, and others to be a relevant prototype for quantum chaotic behavior. A further conjecture by Porter and Thomas[5] established the probability distribution to be expected for intensities related to a typical chaotic wave function: χ_ν^2. This is a function that gives the probability distribution of intensities $I/\langle I\rangle$, over the spatial support of the wave function at a given energy ($\langle I\rangle$ is the corresponding mean value). Later on, Dyson demonstrated that the parameter ν can take only three different values (i.e., 1, 2, and 4, depending on the Hamiltonian to be constructed with real, complex, or quaternions numbers). On the other hand, starting from a semiclassical analysis, Berry suggested that a typical wave function for a chaotic system could be formed by an infinite superposition of plane waves traveling in random directions and with random phases.[6] Working with this important conjecture, Berry was able to show that the probability distribution for those wave functions is $P(I/\langle I\rangle) = e^{-I/\langle I\rangle}$, with $I=\psi\psi^*$, and that the space-averaged spatial correlation of the wave function (at a fixed energy) is proportional to the zeroth-order integer Bessel function. Finally, the application of a supersymmetry formalism has produced a rigorous deduction of the probability distributions associated with a nonlinear supermatrix σ model,[7] which under certain assumptions can be shown to be equivalent to RMT and results in the Porter-Thomas distribution.[8]

It is clear that RMT bears some limitations, derived particularly from its statistical nature. However, it has the advantage of providing an unequivocal object to be studied and a corresponding well defined methodology. In this paper we adopt this statistical approach and having in mind the results from RMT, we study the probability distributions associated with wave functions relevant for popular surface structure techniques, such as low-energy electron diffraction (LEED) or x-ray photoelectron diffraction (PED). Wave functions potentially provide more information than the mere inspection of levels and are also the natural objects to be studied in these scattering techniques. We find that the computed probability distributions match closely the statistics of the eigenfunctions of a Hamiltonian belonging to the Gaussian unitary ensemble (GUE). This is the universality class relevant to a scattering experiment, i.e., to an open geometry, where the energy takes values in the continuum (good quantum numbers characterizing the wave function are the energy and $k_\parallel$ to the surface). Therefore, we take a fresh look at the physical system and advance the hypothesis that the good structural sensitivity of these techniques can be also understood as a manifestation of quantum chaos on the wave functions. This conjecture is tested for two standard correlation factors widely used to measure the *distance* between a reference structure (usually the experimental one) and a trial one calculated theoretically. The results point in the same direction as the statistical analysis of wave functions since we find that there is a region where the correlation factor grows at an exponential rate.

Even if our analysis is not directly linked to classical physics, it is worth mentioning that for every quantum system we have considered its classical analog behaves chaotically due to the intrinsic complexity of the many-scatterer problem.[6,9] As the classical problem might behave chaotically even if the scatterers are regularly distributed, it is surprising to find such a vast literature on quantum chaos related to some kind of disorder, but such little consideration of ordered systems because, using the classical analog to guide intuition, it is not clear why quantum chaos should not to be found in perfectly ordered systems. Recently, Mucciolo *et al.*[10] have shown that the high-energy region of the calculated band structure of crystalline Si is complex enough to

follow the statistical distribution of levels expected for the Gaussian orthogonal ensemble universality class. Inspired by these ideas, we have also presented a preliminary work studying the statistical properties of LEED states[11] on ordered materials. Of course, the LEED problem is related to the band structure analysis, its main advantage being merely practical, because of the readily available experimental data to test theoretical findings.

Berry has studied the Sinai billiard by mapping the problem to a periodic array of hard circles on a plane.[12] This problem can be solved efficiently applying a Korringa-Kohn-Rostoker formalism. His method not only has a number of computational advantages, but also allows a detailed analysis for the different role played by nonisolated and isolated orbits contributing to the wave functions. It is interesting to notice that the nonisolated orbits add to the complexity of the system only through the boundaries defining the billiard. Therefore, although their role is non-negligible to the determination of the chaotic nature of the levels in the closed system, they do not contribute to the open problem of scattering. In other words, paths that never strike a disk do not contribute to the reflectivity of a surface (like in LEED) or they are deliberately removed from the analysis [like in PED or diffuse LEED (DLEED)] due to their lack of useful structural information. In scattering experiments, these paths would be characterized by a probability distribution given by χ^2_∞ (a Dirac's δ function). Therefore, the study of an open system allows one quite naturally to separate the influence of nonisolated and isolated orbits because the nonisolated ones yield only a trivial contribution, in contradistinction to the essential entanglement between both types in the bound problem.

The organization of this paper is as follows. The scattering of a plane wave by an ordered array of hard-sphere potentials is analyzed in Sec. II by applying a LEED formalism. This is a good analog to Berry's work on Sinai's billiard from a scattering point of view, although some important differences remain (e.g., it is a genuine three-dimensional system). The hard-sphere model is interesting from a theoretical point of view because of the strong similarity with the billiard problem and also because its analysis uses the same basic tools employed in the solution of the diffraction by a surface. Certainly, the usual approach to the LEED problem[13] starts by computing the diffraction matrices for a single layer and then proceeds by stacking layers by different methods. In practice that means solving first the multiple scattering problem *inside* a layer and then the multiple-scattering problem *between* layers through a stacking process that finally recreates the material bulk, or at least a thick enough slab. The use of hard-sphere potentials simplifies the computational problem, allowing the identification of the key physical elements responsible for the appearance of the Porter-Thomas probability distribution. Following the strategy of introducing the complexity step by step, we start by computing the reflection and transmission matrices for one layer of hard-sphere potentials. Those layers are then stacked to form a fcc crystal with an arbitrary lattice parameter borrowed from copper. Section III gives a similar analysis for a LEED problem trying to represent realistically a few selected materials. Results corresponding to both DLEED and conventional $I(E)$ analyses are discussed. Finally, we consider in Sec. IV the impact of our previous findings on the statistical correlation factors (R factors) widely used in LEED or PED to assess the confidence on a structure predicted by theory. This is usually done by a trial and error fit, comparing theoretically calculated diffracted intensities with the experiment. The usual rules are as simple as (i) the lower the R factor the better and (ii) the R factor should represent a (hopefully global) minimum. In practice, because there is no way to secure a real global minimum in a multidimensional parameter space, the recipe of getting a low-enough value becomes the only guide to trust or not a given structure. We shall see how a new criterion adding to the others can be obtained by identifying the existence of a region where the R factor changes quickly (exponentially) from values typically obtained from the application of perturbation theory ($R \approx 0$) to values representative for uncorrelated intensities ($R \approx 1$). We argue that this exponential dependence is a consequence of the chaotic nature of wave functions obtained in a complicated multiple-scattering scenario.

II. SIMPLIFIED MODEL OF ELECTRON MULTIPLE SCATTERING BY AN N SCATTERER: HARD-SPHERE POTENTIALS

A. Scattering by an isolated potential

We analyze first the simplest case related to our problem: the scattering of a plane wave e^{ikz} by a single atomic potential modeled by a hard-sphere of radius R.[14] The scattered wave is given asymptotically by

$$e^{ikz} + f_k(\theta)\frac{e^{ikr}}{r}, \tag{1}$$

with

$$f_k(\theta) = \frac{1}{k}\sum_{l=0,\infty} \sqrt{4\pi(2l+1)}\, t_l(k) Y_{l0}(\theta), \tag{2}$$

where

$$t_l(k) = e^{i\delta_l}\sin(\delta_l)$$

and[15]

$$\delta_l(k) = \arctan\left[(-1)^{l-1}\frac{J_{l+1/2}(kR)}{J_{-l-1/2}(kR)}\right].$$

The hard-sphere potential can be compared with a realistic one representing a Ni atom by computing the total scattering cross section. As an example, at an intermediate energy such as $E=5$ a.u., this cross section is about 20% less for a hard sphere having $R=1$ a.u. than for the Ni atom, while for $R=2$ a.u. it becomes three times bigger.

Figure 1 displays the probability distribution function for intensities scattered by this model at constant energy when the angle θ is varied. This is compared with the Porter-Thomas law characteristic of a chaotic system to stress the different statistical behavior. Only two parameters are relevant to this experiment: the length scale ($R=2$ a.u.) and the energy scale. The approximate semiclassical rule $kR \approx l_{max}$ gives us some rough value for the maximum component in the spherical wave expansion, and twice that value is used in all our calculations ($l_{max}=20$). Because the phase

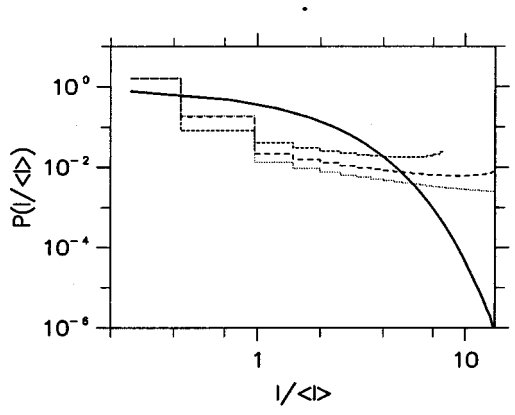

FIG. 1. Probability distribution for the scattering of a plane wave by a single hard-sphere potential ($R=2$ a.u.). Three energies (in a.u.) are shown: $E=2$ (short-dashed line), $E=5$ (long-dashed line), and $E=10$ (dotted line). The thick solid line is the χ^2_2 function corresponding to the GUE wave-function statistics.

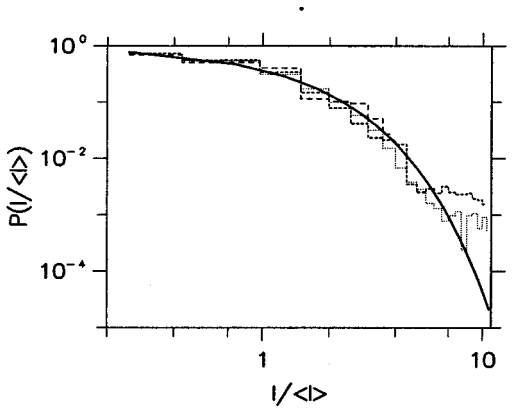

FIG. 2. Probability distribution of wave functions reflected by one layer of hard-sphere potentials. Results for $R=2$ a.u. and three different energies are shown: $E=2$ a.u. (long-dashed line), 5 a.u. (short-dashed line), and 10 a.u. (dotted line).

shifts bring some nontrivial dependence on kR through the spherical Bessel functions, the results for three different energy values spanning the range of interest are given to illustrate this dependence. Basically, the same statistical pattern is found, reflecting the smooth variation of the scattering factor (modulated by the forward peak). This probability distribution is remarkably similar to the one found for the typical wave function of a chaotic system when too few random components are used.[11]

B. Electron diffraction by a plane of scatterers

The same statistical probability distribution is expected for the diffraction of a single Bravais lattice in the kinematic approximation at normal incidence, where all the atoms scatter the plane wave at the same time and are equivalent because of the Bravais-like symmetry. In this approximation, the lattice is merely contributing a structure factor composed of δ functions centered around Bragg conditions.[16] However, by taking an appropriate limit on the full dynamical result, we shall see that this is not the case when the angle of incidence is varied (cf. Fig. 4) because of the $n\sin(\theta)$ extra path added to each scatterer in the plane ($n=0,\infty$).

To proceed gradually from simple to more complicated systems, we now analyze the diffraction matrix of a single two-dimensional Bravais lattice[13,16,17]

$$M_{\vec{K}^{\pm}_{\vec{g}'},\vec{K}^{\pm}_{\vec{g}}}=\frac{8\pi^2 i}{|\vec{K}^{\pm}_{\vec{g}}|\vec{K}^{\pm}_{\vec{g}',z}}\sum_{l,m;l',m'} e^{i\delta_{l'}}\sin(\delta_{l'})\times\{i^{l}(-1)^{m}Y_{l-m}(\vec{K}^{\pm}_{\vec{g}})\}\times\frac{1}{(1-X)_{lm,l'm'}}\{i^{-l'}Y_{l'm'}(\vec{K}^{\pm}_{\vec{g}'})\}. \quad (3)$$

This expression gives the complex amplitude diffracted from an ingoing beam $\vec{K}^{\pm}_{\vec{g}}$ into an outgoing one $\vec{K}^{\pm}_{\vec{g}'}$. Therefore, it is the basic quantity needed to compute the reflection $R=M^{+,-}$ and transmission $T=I+M^{+,+}$ of just one layer (a minus sign denotes propagation towards the vacuum where the original wave was originated and a plus sign propagation in the opposite direction).

Figure 2 shows the wave-function statistical distributions obtained for a two-dimensional square lattice of hard-sphere potentials at nearest-neighbor distances taken from a Cu(100) surface (4.82 a.u.). Internal parameters relevant for the calculation are kept to the same values as the preceding case ($R=2$ a.u. and $l_{max}=20$). An arbitrarily small positive imaginary part V_{0i} is added to the energy to give the Green's functions the required analytical behavior. The physical effect of such a mathematical trick is to ensure the proper decay of waves at infinity. The actual value used in our calculations is $V_{0i}=0.001$ a.u., small enough compared with all relevant energies as not to have any noticeable effect (Kambe's method[18] is used to compute the lattice summation and about 2300 lattice points are included). Given these values for the internal parameters of the model, intensities still depend on external parameters that typically will be explored in real experiments: the energy and the incident and collection angles. In our previous work[11] we have studied the statistical probability distribution in scattering intensities varying the collection angle (DLEED) and the energy [standard $I(E)$ LEED analysis], but at a fixed incident angle defined by θ and ϕ. In this paper we increase the database size by considering different initial incident directions on a solid angle centered around $\theta=0°$ and $30°$–$40°$ wide. As the energy is the main external parameter controlling the experiment, the results for three different energies spanning the range of interest ($E=2$, 5, and 10 a.u.) are systematically shown for comparison. We remark that the trivial limit χ^2_∞ is recovered at fixed energy from Eq. (3) for $l_{max}=0$ or, alternatively, when $R\to 0$, which eventually would make only one spherical component necessary, eliminating the dependence on the angle θ or ϕ. All the parameters used in our model correspond to realistic values used in real LEED experiments, except for the very small imaginary part for the optical potential. In a typical LEED experiment the inelastic interaction is strong, concentrating the diffraction process on the vicinity of the surface (which explains the sensitivity of the experiment to small atomic displacements in the last few layers). This can be taken into account effectively by includ-

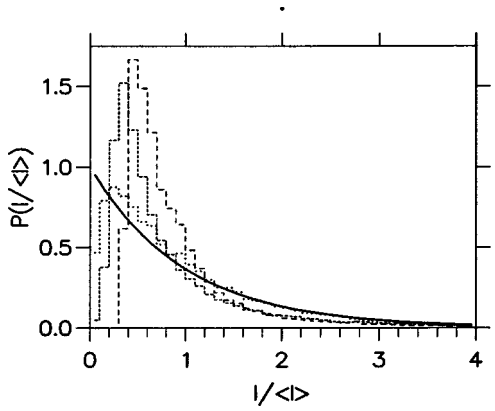

FIG. 3. Dependence of the wave-function probability distribution on the hard-sphere radius. Results for $E=10$ a.u. and $R=2.0$ a.u. (dotted line), 0.2 a.u. (dashed line), and 0.02 a.u. (long-dashed line) are shown.

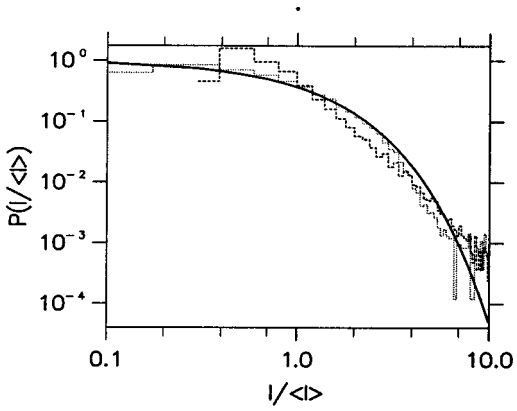

FIG. 4. Full dynamical model for a single Bravais lattice (dotted line) compared to a kinematic one (dashed line). The parameters for the calculation are $E=10$ a.u., $R=2$ a.u., and $l_{max}=20$.

ing a large optical potential ($\approx 0.1-0.2$ a.u.) in the energy. However, it is important to realize that the experiment is conceived as purely elastic and electrons having lost some energy do not contribute to the detected intensity. Realistic values have been used previously to make contact with experiments[11] and now we are more interested in isolating the physical effects related to a complex behavior. Therefore, we choose to work in the limit $V_{0i}\rightarrow 0$ to minimize the effect of this value and we shall discuss the role of this parameter in more detail in Fig. 6. The actual computer code used is a modern version of routines given by Pendry.[13] Figure 2 clearly shows how the single Bravais layer gives diffracted intensities that already have statistical distributions close to the ideal Porter-Thomas law, irrespective of the energy.

Next, the energy is fixed at some arbitrary representative value ($E=10$ a.u.) and the dependence of the statistical probability distribution of a two-dimensional Bravais lattice on the size of the hard-sphere potential is studied. Figure 3 gives the statistics for three different sizes of the hard-sphere radius. As $R\rightarrow 0$, the reflected intensities also become negligible. From a computational point of view, we do not expect this limit to be strictly accessible for a numerical experiment because the computer zero, determined by a numerical underflow, might be contaminated by roundoff errors with a statistical distribution not know *a priori*. Average values for the intensities at $E=10$ a.u. are 1.6×10^{-2}, 2.5×10^{-4}, and 4.1×10^{-6}, respectively, for $R=2$, 0.2, and 0.02 (a.u.). Figure 3 shows the tendency of the probability distribution towards χ^2_∞, associated with the constant value corresponding to a very small radius value. As the main interest in this case is to show the behavior near the origin, we have skipped the usual log-log plot, well suited to manifest the fast exponential decay, but not so useful to stress the behavior near the origin.

To understand the role of the complexity created by the intralayer multiple scattering versus the geometrical factor of different incident angles, we have artificially made the intralayer scattering matrix equal to zero: $X=0$. The result is shown in Fig. 4 for fixed values of E, R, and l_{max}. It is observed that the kinematic N-scatterer problem analyzed for different incident angles already approximates the Porter-Thomas distribution, although the inclusion of intralayer multiple scattering gives a distribution closer to the ideal one.

C. Electron diffraction by a stacking of planes of hard-sphere scatterers

We use the *layer doubling* scheme[13] to stack layers of hard-sphere potentials. Layers are stacked to form a fcc lattice, borrowing the intralayer distances from copper, as before. Taking into account the small imaginary part used in our calculations, we should at least double the width of the slab up to distances of about $l_c\approx\sqrt{2E}/V_{0i}$, approximately including 1000 layers. This is not practical, or necessary, and we only slowly double the slab size to investigate the influence of the layer width on the statistical distribution.

This is illustrated in Fig. 5 for four different widths: 2, 4, 8, and 16 layers (for comparison, the result for 1 layer can be found in Fig. 4). Other parameters are fixed to the same values previously used to isolate features only associated to the slab width. It is easily appreciated how the statistical distribution tends more to behave like the ideal Porter-Thomas one as the width is increased. It is difficult to math-

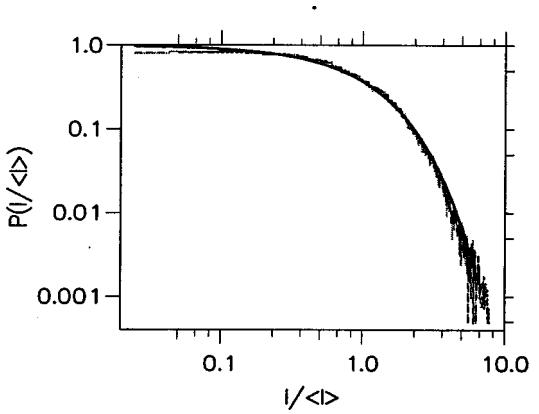

FIG. 5. Reflected intensities statistics of a full dynamical calculation of a slab of increasing width: The numbers of stacked layers are 2 (dotted line), 4 (dashed line), 8 (long-dashed line), and 16 (double-dash–double-dotted line). Other computational parameters are given in Fig. 4.

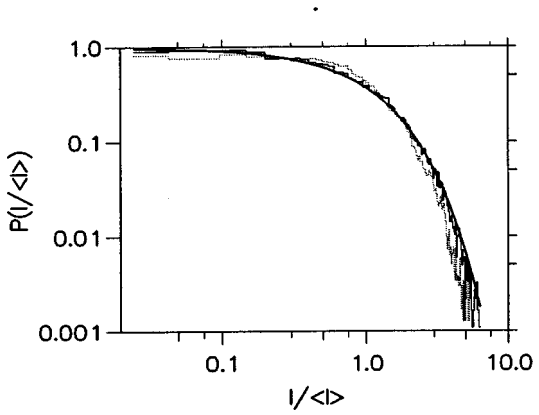

FIG. 6. Probability distributions for a 16-layer slab for different imaginary parts added to the energy: $V_{0i}=0.001$ a.u. (thin continuous line) and $V_{0i}=0.1$ a.u. (dotted line). Other computational parameters are given in Fig. 4.

ematically quantify this tendency, but an approximate way would be to make a least-squares fit of the data to χ^2_ν functions and give the ν with the best agreement. This results in $\nu=2.7$, 2.3, 2.2, 2.2, and 2.2 for 1, 2, 4, 8, and 16 layers, respectively. The mean values of the intensity reflected are for each case 1.58×10^{-2}, 2.42×10^{-2}, 2.55×10^{-2}, 2.58×10^{-2}, and 2.58×10^{-2}. A penetration depth of 16 layers is thought to be a practical upper limit for most experimental systems. From these numbers it must be concluded that, at least under the particular conditions we have chosen, *intralayer* scattering between the first two layers helps the distribution most to compare well with the Porter-Thomas law, while further stacking of layers mainly contributes to improve the finer details. Therefore, a moderate amount of multiple scattering should be generically held responsible for the statistical behavior of wave functions, characteristic of quantum chaos.

The main role of the imaginary part added to the energy V_{0i} is to attenuate the wave field, as can be understood by reference to the underlying Green's functions used in the theory. Waves dying out with some characteristic length serve to mimic inelastic effects that can take away current from the pure elastic experiment considered in LEED theory. Large values of V_{0i} imply waves decaying faster with distance and making the system less *complex* because the number of multiple scattering events is effectively reduced. This is the effect observed in Fig. 6, where, using the same parameters as in Fig. 5, we have compared the results for $V_{0i}=0.001$ and 0.1 a.u. The agreement between the ideal Porter-Thomas distribution and the different simulations considered degrade systematically with larger values of V_{0i}, as can be seen from a least-squares fit giving $\nu=2.2$, 2.2, 2.4, and 2.7 for $V_{0i}=0.001$, 0.01, 0.1, and 0.2 a.u., respectively. These numbers range from the very small values (0.001 a.u. is associated with a decaying length of thousands of angstroms) to the few eV used in standard structural analysis (0.2 a.u. is associated with a decaying length of tenths of angstroms). This discussion should make clear that the probability distributions found here, representative of quantum chaos, do not originate in inelastic or many-body effects represented by a complex self-energy, but are only due to complexity driven by the multiple-scattering scenario.

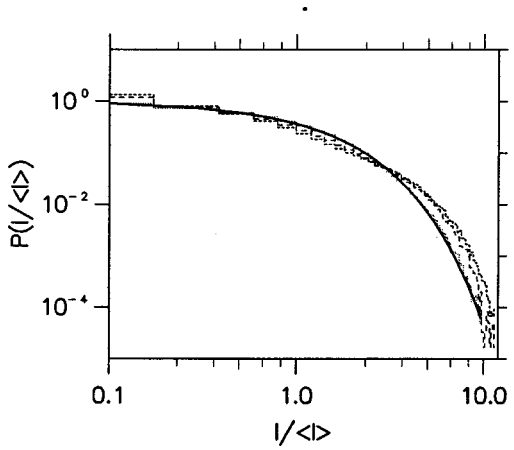

FIG. 7. Probability distribution for DLEED intensities of O/Ni(100). $E=12$ a.u. (dotted line), 14 a.u. (short-dashed line), and 16 a.u. (long-dashed line).

III. APPLICATION TO DIFFUSE AND CONVENTIONAL $I(E)$ LEED ANALYSIS

All these ideas can be used to analyze LEED experiments conducted in standard surface structural analysis. Those experiments are performed by measuring as a function of the energy the available exiting beams [$I(E)$ standard LEED] or by analyzing many different exiting beams at a few fixed energies (DLEED). The former technique is usually applied to ordered surfaces, while the latter is more appropriate to surfaces with disorder. As the relevant physical principles behind LEED and DLEED are well described by a multiple-scattering formalism, it is not surprising to find that both intensities simulated theoretically for realistic systems and the corresponding to values measured experimentally fit rather well the Porter-Thomas distribution. Indeed, the main differences from our previous model are the atomic potentials and the important electron-electron inelastic interaction that attenuates the wave within a few layers of the surface. While our results are not very sensitive to a particular set of phase shifts, as becomes obvious from our results for different materials simulated with realistic potentials, the influence of a large optical potential is balanced by our finding that scattering by one or two layers at most is enough to reproduce the characteristic GUE probability distribution.

This is demonstrated in Figs. 7–11. We first explore the statistical behavior of DLEED. A representative system considered many times in the literature from both the experimental and the theoretical point of view is the lattice gas disordered adsorption of oxygen on Ni(100).[19] Nickel is obviously a strong scatterer and multiple scattering plays an important role. This is relevant because the adsorbate is illuminated directly both by the wave coming from the electron gun and by the reflected wave coming from the surface, which depends on the energy and angle in a complicated manner dictated by the multiple scattering inside the substrate. Geometrical parameters are taken from a detailed structural search, fixing the adsorption position at about 1.5 a.u. on the fourfold symmetry position in the square surface lattice (less symmetric adsorption sites would only make more complex the system and therefore more likely to recover the Porter-Thomas law). Three different energies are computed theoretically using a dynamical approach at T

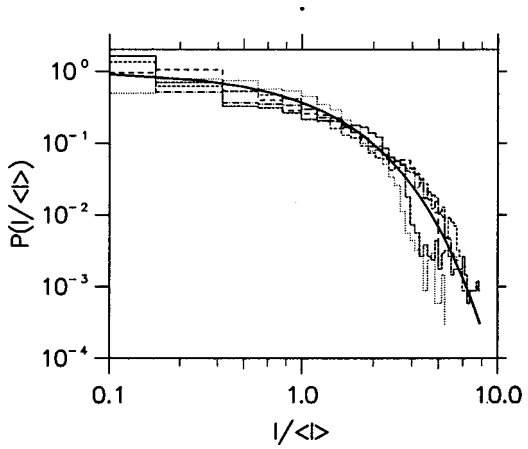

FIG. 8. Probability distribution for experimental DLEED intensities of O/Ni(100). $E=3.7$ a.u. (dotted line), 5.6 a.u. (short-dashed line), 7.5 a.u. (long-dashed line), 9.4 a.u. (long-dash–dotted line), and 11.1 a.u. (long-dash–short-dashed line).

$=0$ K, as described by Saldin and Pendry.[20] To improve the statistics, different incident angles θ and ϕ are computed and used as explained above. The agreement with the Porter-Thomas law is quite good (e.g., $E=12$ a.u. gives a least-squares fit ν value of 2.0), reflecting that although the diffuse background is generated by scattering with only one atom responsible for breaking the otherwise perfect symmetry that would result in Bragg conditions, the wave reflected by the substrate and illuminating the atom is very complicated. Obviously what matters most here is that the forward scattering of that wave by the adsorbate is stronger than or comparable to the backscattering of the simple plane wave by the same potential.

Our previous findings can also be corroborated by analyzing experimental DLEED intensities measured for the same system by the Erlangen group.[21] Figure 8 shows such an analysis for five different energies going from $E=3.7$ a.u. to $E=11.1$ a.u. in approximate steps of 1.8 a.u. The database was measured in a sample cooled down to liquid-nitrogen temperature (≈ 90 K), at normal incidence, and for an approximate coverage of 0.25 (1 representing one full monolayer adsorbed). Less than one-thirtieth of the amount of data used in the theoretical analysis is available, making a poorer statistics, but the expected tendency is followed well, although fluctuations are clearly observed.

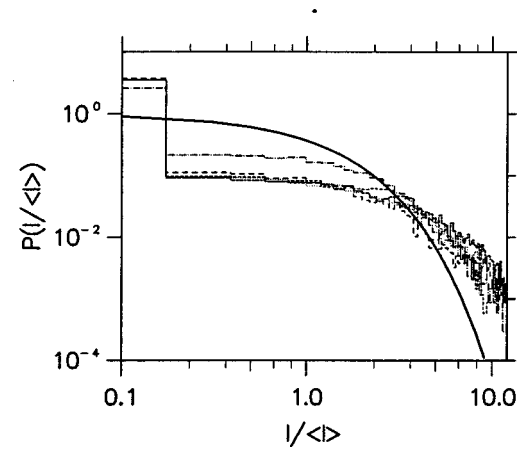

FIG. 9. Probability distribution for experimental DLEED intensities of K/Ni(100). $E=3.7$ a.u. (dotted line), 5.6 a.u. (short-dashed line), 7.5 a.u. (long-dashed line), 9.4 a.u. (long-dash–dotted line), and 11.1 a.u. (long-dashed–short-dashed line).

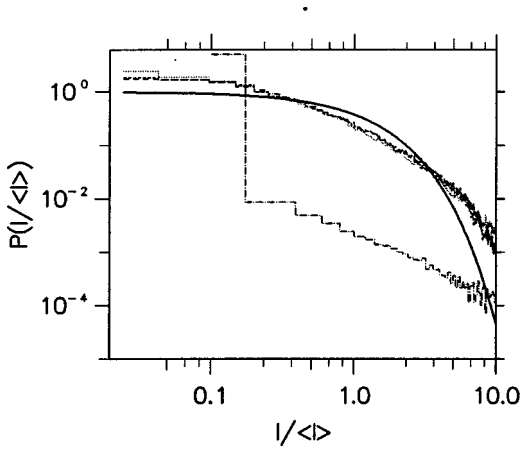

FIG. 10. Probability distribution corresponding to the LEED $I(E)$ curves for Cu(100), considering different surface relaxations, $d_{12}=3.40$ a.u. (dotted line), $d_{12}=3.02$ a.u. (short-dashed line), an equally weighted average from 3.02 to 3.74 (long-dashed line), and $d_{12}=2.00$ a.u. (dash-dotted line).

We have also analyzed the experimental data measured by the Erlangen group on the (disordered) K/Ni(100) system. Normal incidence and liquid-nitrogen cooling ($T=90$ K) are used again. Potassium coverage is kept at a lower value of 0.05. This system, however, shows an important difference from the last one: Potassium is adsorbed at the hollow site, but at a much higher position, ≈ 5.1 a.u. It is clear that the source of complexity is the substrate, and if the atom would be isolated, or too far away from the surface, the DLEED intensities would simply correspond to the ones due to a single atomic potential. From our previous estimate for the typical decaying length, we find that $l_c \approx 15-20$ a.u. for the energies involved in the experimental data. Therefore, it is not unexpected that the probability distribution for K/Ni(100) bears some similarity to the one obtained for an isolated atom, as can be seen in Fig. 9.

By reference to the RMT or to Berry's hypothesis about

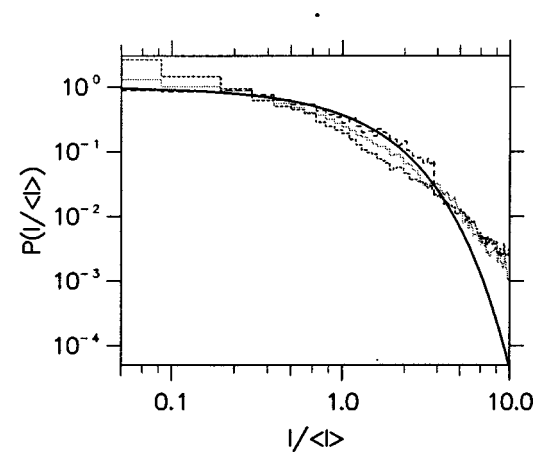

FIG. 11. Probability distribution corresponding to the LEED $I(E)$ curves for W(100) (dotted line), Si(111) (dashed line), and $c(8\times 2)$-GaAs(100) (long-dashed line).

the structure of the typical wave function of a chaotic system, it is clear that the same Porter-Thomas law should manifest if intensities are analyzed as a function of energy at a fixed arbitrary position $\vec{r}$. We have analyzed this behavior for scattering wave functions by calculating LEED $I(E)$ curves for three materials not bearing a structural or an electronic relationship, Cu(100), W(100), and Si(111), and by analyzing a real LEED experiment. Figure 10 shows the probability distributions computed for Cu(100) and Fig. 11 gives the same result for W(100), Si(111), and experimental data for $c(8\times2)$ GaAs(100). The Van Hove–Tong LEED package is used to compute intensities within the renormalized forward scattering (RFS) approximation to describe multiple scattering between layers and realistic phase shifts representing the atomic potentials are considered.[22] To improve the statistical confidence of the results, we choose an arbitrary azimuthal angle (not related to any symmetry direction) of $\phi=30°$ and explore a range of polar angles from $\theta=5°$ to $\theta=40°$, in steps of $\theta=5°$. The first nine emergent beams over an energy range from $E=2$ to 20 a.u. are considered and other parameters relevant for the calculation are $l_{max}=7, V_{0i}=0.15$ a.u., $T=0$ K, and up to a maximum of 101 beams included. For copper, we consider two different distances between the first and the second surface layers, $d_{12}=3.4$ a.u. and 3.02, corresponding, respectively, to the perfect unrelaxed surface and to the experimental relaxation found on clean Cu(100) crystals. Both cases are seen (cf. Fig. 10) to be well represented by the χ^2_2 probability distribution. An average of intensities for different samples with d_{12} values going from 3.02 to 3.74 in steps of 0.08 a.u. is also considered with a similar result. In addition, we compute a hypothetical relaxation of $d_{12}=2.0$ a.u., where the RFS technique is used outside its validity region and it results in unphysical divergences. The statistical distribution associated with this absurd case is seen to be very different from the previous ones, signaling clearly that something went wrong in the calculation. This is an extreme situation, but the same we have been able to detect a theoretical problem with a simple statistical analysis; the Porter-Thomas distribution may help to identify cases where gross experimental systematic errors, such as an improper subtraction of the background or saturation of some bright beams, occur. We have repeated a similar theoretical analysis for W(100) and Si(111) surfaces in Fig. 11. While similar conditions are used for W(100), owing to experimental practical difficulties to measure the high-energy end in semiconductors, we use a smaller energy range for Si(111) (from 1 to 11 a.u.), but the first 13 emerging beams are considered to have a database with a similar size to the one considered for the metals.

Although agreement between the multiple-scattering calculations and experimental data is very good for geometries representing well a given surface [e.g., the Pendry R factor for the structural analysis of Cu(100) is already below 0.1 and experimental and theoretical $I(E)$ curves are hardly distinguishable by simple ocular inspection], we also take into account experimental intensities from the $c(8\times2)$-GaAs(100) reconstruction.[23] Nineteen independent beams measured at normal incidence and giving an approximated energy range of 86 a.u. are considered. Intensities have been digitalized from the published results and interpolated with splines in such a way that the interpolated curves cannot be distinguished by eye from the measured data. Again, fair agreement between the obtained probability distributions and the ideal Porter-Thomas law is obtained, although we observe that the agreement is achieved over a limited range due to the smaller amount of available data.

IV. *R*-FACTOR DEPENDENCE ON GEOMETRICAL STRUCTURAL PARAMETERS

An interesting question derived from the chaotic nature of the wave function is how quickly two given structures differing in a given structural parameter p become unrelated from the point of view of diffracted intensities. This process happens, although the two structures are always related through some underlaying geometrical relationship, via the complexity introduced by multiple scattering. To investigate this point, we first analyze theoretically computed diffracted intensities where only one relevant parameter is varied. Afterward, we apply the same ideas to a recent structural search on an experimental system performed by other people.[24] The theoretical experiment is performed using the same DLEED program mentioned before.[20] This allows us to simulate the adsorption of an oxygen atom on the hollow site of a perfect (unrelaxed) Ni(100) surface. The reference height is fixed again at 1.5 a.u. from the layer defined by the nickel cores, which is very similar to the experimental value. Changing the oxygen adsorption height, we study the corresponding changes in the DLEED intensities. We notice that the same code has been used previously for a real structural search on this system, proving its capability to give a realistic description of the physical system.[19]

To measure the changes in the LEED diffracted intensities we adopt two common but otherwise unrelated correlation factors: (i) the root mean square deviation R_{RMSD} (Ref. 16) and (ii) the Pendry R factor R_P.[25] The former is the simplest choice at hand and we apply it to the DLEED theoretical experiment:

$$R_{RMSD}=\sqrt{\frac{1}{N}\sum_{k=1,N}(I_k^{ref}-I_k)^2}, \tag{4}$$

where k labels the different $\vec{k}_{\parallel,out}$. This R factor is conveniently normalized to $1/\sqrt{N}$, the value expected for two random sets of intensities with the same average value (intensities are normalized to their average value). On the other hand, the Pendry R factor is a very common choice in standard structural analysis of $I(E)$ LEED curves and because it was used by Polop *et al.*[24] in their study of $c(2\times2)$ Si/Cu(110), we simply analyze the behavior of their published values. The fact that we find the same type of behavior with two so different R factors supports our hypothesis that the effects discussed in this section are quite general.

We distinguish the existence of three different regions in parameter space P: I, a perturbative region, characterized by a polynomial dependence $R(p)\propto p^n$; II, an exponential region $R(p)\propto e^p$, where small changes in a given structural parameter result in rapidly increasing R values; and III, a fully chaotic region where the R factor saturates approximately to the values expected for the comparison between two randomly generated structures (by definition ≈1 in both R factors used here). Beyond these regions, the existence of

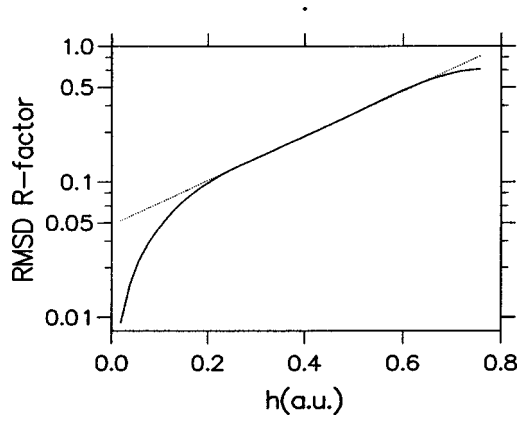

FIG. 12. Root mean square deviation (R_2) measuring the correlation between a reference structure $S(0)$ and a family of structures labeled by the adsorption height of an atom $S(h)$. Region II (see the text) is shown as the linear region (in logarithmic scale) between the minimum (region I) and the saturation region (region III). Energy is fixed to 2.0 a.u.

diffraction multiple coincidence minima recreates again similar although more imperfect conditions.[26] The existence of region I is justified by the applicability of perturbative techniques (given a sufficiently small perturbation). This would result in a series expansion in terms of the parameter p and the polynomial dependence. How small the perturbation should be can be estimated by applying some simple version of perturbation theory. As an example, take tensor LEED in its first form, where the change in the scattered amplitude is proportional to the change in the potential. For the simpler version, where the change in the potential is linearly related to the change in the atomic position, the range of validity is known by common experience on different systems to be ≈ 0.2 a.u.[27] A renormalized form of this theory, where the change in the amplitude is proportional to the change in the t matrix, is generally accepted up to ≈ 0.8 a.u., but we notice that it already implies adding up an infinite series in the potential, going beyond the straight application of perturbation theory. Those displacements correspond typically to R factors between the reference structure (by definition $R=0$) and the one to be computed perturbatively of about $R=0.2-0.4$. In the examples presented below (Figs. 12 and 13), we observe that this normally corresponds to a region where the R factor changes exponentially with the structural parameter. Therefore, it is possible to understand why perturbation theory breaks around this region II, in spite of the considerable effort that has been made to write the change in the amplitude as a power series of the atomic displacement.[28]

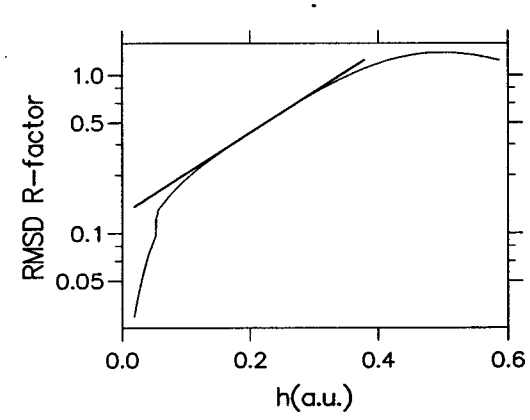

FIG. 13. Same results as presented in Fig. 12, but for $E=5.0$ a.u.

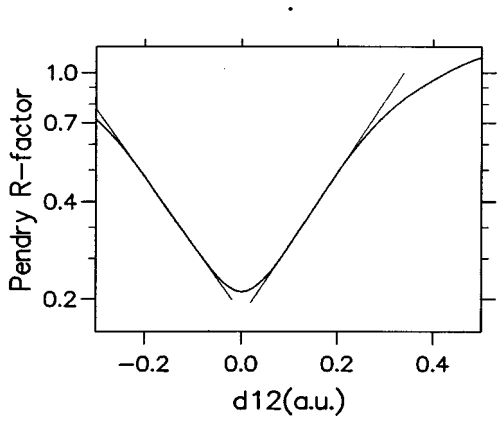

FIG. 14. The Pendry R factor is analyzed in a similar way to R_{RMSD} in Fig. 12. The data corresponding to an experimental structural analysis by $I(E)$ LEED of $c(2\times 2)$Si/Cu(110) are considered.

The existence of region II is illustrated in Figs. 12 and 13 with theoretically simulated data and in Fig. 14 with data produced by comparing with the experiments. Regarding the theoretical simulation, we have slowly increased the adsorption height of the oxygen atom to get a corresponding increase in the R_{RMSD}. To show the functional dependence between R_{RMSD} and h, we take logarithms in the ordinate axis and we identify an interval where the curve can be approximated very well by a straight line. This region should be considered the onset of quantum chaos and therefore a region of dubious value for structural work.

To test whether or not this behavior is particular to a given definition of the R factor, we perform the same analysis using the Pendry R factor. This function is defined in very different terms from the simpler R_{RMSD} considered above. However, Fig. 14 shows the same type of behavior for R_P. This corresponds to R factors comparing structural models to experimental data for a recent structural search performed on the system $c(2\times 2)$Si/Cu(110) using conventional $I(E)$ curves.[24] R_P is studied as a function of the two outer interlayer distances d_{12}, where the best value provided by the structural work has been subtracted to put the origin at $d_{12}=0$.

V. CONCLUSIONS

Scattering intensities have been analyzed from a statistical point of view. The computed probability distributions compare well with the Porter-Thomas law, typical of random wave functions. To understand the origin of such a similarity we have analyzed models with increasing scattering complexity, using a hard-sphere approximation for the interaction potentials. The simplest case found by displaying a statistical distribution similar to the Porter-Thomas law is single scattering by a Bravais lattice of N scatterers at an arbitrary angle of incidence. When more complexity is added to the system (e.g., by considering intralayer multiple scattering or multiple scattering between a few layers through a *layer dou-*

bling stacking strategy), the statistical distribution of such idealized systems shows better agreement with the ideal χ_2^2 function. The same behavior is found if realistic potentials are considered to describe the atoms within the periodic lattice. The analysis of real experimental data is also consistent with the same ideas, as expected from the known reliability of those theoretical methods to give scattering intensities if the geometries are already known. Finally, we have found that standard *R* factors behave exponentially in a transition region II before the intrinsic complexity of multiple scattering effectively decouples wave functions for different geometrical structures. The existence of this region allows us to use concepts borrowed from classical chaos and to propose a criterion for the reliability of a given minimum in the *R* factor, depending on whether the structure lies in a perturbative region I or beyond the transition zone III.

ACKNOWLEDGMENTS

This work has been supported by the CICYT under Contracts Nos. PB96-0085 and PB94-0053. We are grateful to Professor K. Heinz for making available to us the experimental DLEED data.

[1] M. V. Berry, in *Chaos and Quantum Physics*, edited by M. J. Giannoni, A. Voros, and J. Zinn-Justin (Elsevier, Amsterdam, 1991), p. 251.
[2] See, e.g., *Statistical Theories of Spectra: Fluctuations*, edited by C. E. Porter (Academic, New York, 1965).
[3] M. L. Mehta, *Random Matrices*, 2nd ed. (Academic, San Diego, 1991).
[4] T. A. Brody, J. Flores, J. B. French, P. A. Mello, A. Pandey, and S. S. M. Wong, Rev. Mod. Phys. **53**, 385 (1981).
[5] C. E. Porter and R. G. Thomas, Phys. Rev. **104**, 483 (1956).
[6] M. Berry, in *Chaotic Behaviour of Deterministic Systems*, 1983 Les Houches Lectures, Session XXXVI, edited by G. Iooss, R. H. G. Helleman, and R. Stora (North-Holland, Amsterdam, 1983), p. 171.
[7] K. B. Efetov, *Supersymmetry in Disorder and Chaos* (Cambridge University Press, Cambridge, 1997).
[8] V. I. Falko and K. B. Efetov, Phys. Rev. B **52**, 17 413 (1995).
[9] M. C. Gutzwiller, *Chaos in Classical and Quantum Mechanics* (Springer-Verlag, New York, 1990).
[10] E. R. Mucciolo, R. B. Capaz, B. L. Altshuler, and J. D. Joannopoulos, Phys. Rev. B **50**, 8245 (1994).
[11] P. L. de Andres and J. A. Vergés, Phys. Rev. Lett. **80**, 980 (1998).
[12] M. Berry, Ann. Phys. (N.Y.) **131**, 163 (1981).
[13] J. B. Pendry, *Low Energy Electron Diffraction* (Academic, London, 1974).
[14] $\hbar = m_e = e = 1$ is used throughout the paper (i.e., energy is expressed in hartrees, 27.2 eV, and distances in bohrs, 0.0529 nm).
[15] N. F. Mott and H. S. W. Massey, *The Theory of Atomic Collisions* (Oxford University Press, London, 1965).
[16] M. A. Van Hove, W. H. Weinberg, and C. M. Chan, *Low-Energy Electron Diffraction* (Springer-Verlag, Berlin, 1986).
[17] J. L. Beeby, J. Phys. C **1**, 82 (1968).
[18] K. Kambe, Z. Naturforsch. A **23A**, 1280 (1968).
[19] U. Starke, P. L. de Andres, D. K. Saldin, K. Heinz, and J. B. Pendry, Phys. Rev. B **38**, 12 277 (1988).
[20] J. B. Pendry and D. K. Saldin, Surf. Sci. **145**, 33 (1984); D. K. Saldin and J. B. Pendry, Comput. Phys. Commun. **42**, 399 (1986).
[21] K. Heinz (private communication).
[22] M. A. Van Hove and S. Y. Tong, *Surface Crystallography by LEED* (Springer-Verlag, Berlin, 1979).
[23] F. J. Palomares, Ph.D. thesis, Universidad Autonoma de Madrid, 1993, Chap. 3, p. 66.
[24] C. Polop, C. Rojas, E. Roman, J. A. Martin-Gago, B. Brena, D. Cocco, and G. Paolucci, Surf. Sci. **407**, 268 (1998).
[25] J. B. Pendry, J. Phys. C **13**, 937 (1980).
[26] S. Andersson and J. B. Pendry, Solid State Commun. **16**, 563 (1975).
[27] P. J. Rous, J. B. Pendry, D. K. Saldin, K. Heinz, K. Müller, and N. Bickel, Phys. Rev. Lett. **57**, 2951 (1986); P. J. Rous, Ph.D. thesis, Imperial College of Science, Technology and Medicine, London, 1986, Chap. 6, p. 167.
[28] W. Oed, P. J. Rous, and J. B. Pendry, Surf. Sci. **273**, 261 (1992).